THE JOURNAL OF PHYSICAL CHEMISTRY C

Subscriber access provided by UNIV OF HOUSTON

Article

Electric Potential Stability and Ionic Permeability of SAMs on Gold Derived from Bidentate and Tridentate Chelating Alkanethiols

Wei Wang, Shishan Zhang, Pawilai Chinwangso, Rigoberto C. Advincula, and T. Randall Lee

J. Phys. Chem. C, **2009**, 113 (9), 3717-3725• DOI: 10.1021/jp808957r • Publication Date (Web): 06 February 2009

Downloaded from http://pubs.acs.org on April 15, 2009

More About This Article

Additional resources and features associated with this article are available within the HTML version:

- Supporting Information
- Access to high resolution figures
- Links to articles and content related to this article
- Copyright permission to reproduce figures and/or text from this article

View the Full Text HTML

ACS Publications
High quality. High impact.

The Journal of Physical Chemistry C is published by the American Chemical Society. 1155 Sixteenth Street N.W., Washington, DC 20036

Electric Potential Stability and Ionic Permeability of SAMs on Gold Derived from Bidentate and Tridentate Chelating Alkanethiols

Wei Wang, Shishan Zhang, Pawilai Chinwangso, Rigoberto C. Advincula,* and T. Randall Lee*

Department of Chemistry, University of Houston, 4800 Calhoun Road, Houston, Texas 77204-5003

Received: October 9, 2008; Revised Manuscript Received: December 31, 2008

The interfacial electrochemical properties of self-assembled monolayers (SAMs) on gold derived from a structurally tailored series of monodentate, bidentate, and tridentate chelating alkanethiols were investigated. Specific adsorbates included 1-hexadecanethiol (**C16**), 2-tetradecylpropane-1,3-dithiol (**C16C2**), 2-tetradecyl-2-methylpropane-1,3-dithiol (**C16C3**), 2,2-ditetradecylpropane-1,3-dithiol (**C16C16**), and 1,1,1-tris(mercaptomethyl)pentadecane (**t-C16**). Reductive desorption of the SAMs as a function of potential was probed by voltammetric measurements, which indicated the following relative order of electric potential stability: **t-C16** > **C16C2** ≈ **C16C3** ≈ **C16C16** > **C16**. The ionic permeability was investigated under various applied cathodic potentials by electrochemical impedance spectroscopy (EIS). An examination of SAMs prepared at room temperature and accessed by EIS at open-circuit potential showed that the ionic permeability increased in the order **C16C2** < **C16** < **C16C3** < **C16C16** < **t-C16**. The ionic permeability of films was further influenced by the electric potential of the metal substrate and the temperature at which the monolayers were assembled. The potential dependence of the ionic permeability was qualitatively rationalized by considering both the initial ionic permeability and the electric potential stability of the SAMs. Similarly, the ionic permeability of the SAMs prepared at elevated temperature showed contributions from both their thermal stability and their insulating properties at room temperature.

Introduction

Self-assembled monolayers (SAMs) with submaximal packing densities have been interesting topics in interfacial chemistry for decades, largely due to their unique conformational flexibility.[1−11] In contrast to densely packed SAMs that exhibit semicrystalline order, loosely packed SAMs are sterically unencumbered and conformationally disordered. These features offer advances in the development of certain technological applications, including reversible surfaces via electric potential control[2] and dynamic surfaces that are highly resistant to protein adsorption.[10,11]

Quantitative control of packing density has proved to be a challenging objective in the preparation of loosely packed SAMs, even though a variety of strategies have been used to target the problem.[2−11] Furthermore, the generation of highly stable SAMs on gold remains an important challenge for coatings applications[12−14] and patterning via soft lithography.[15,16] Perhaps these objectives have been most capably met by using tailor-made bidentate and tridentate chelating alkanethiols, which provide a systematic control of packing density through the variation of alkyl-to-sulfur ratio and modification of the alkyl group near the quaternary (or "spiro") carbon center.[17−23] Representative bidentate and tridentate thiols include 2-monoalkylpropane-1,3-dithiol (**C*n*C2**), 2-alkyl-2-methylpropane-1,3-dithiol (**C*n*C3**), 2,2-dialkylpropane-1,3-dithiol (**C*n*C*n***), and 1,1,1-tris(mercaptomethyl)alkane (**t-C*n***), as shown in Figure 1. Studies have shown that SAMs prepared from these chelating adsorbates exhibit substantially enhanced wettabilities and frictional properties.[17−19] In addition, the stability of the SAMs is enhanced due to the chelate effect and the energetically disfavored formation of cyclic disulfides.[20] Furthermore, unsymmetrical chelating thiols can be used to prepare homogeneously mixed SAMs at the molecular level.[21]

SAMs derived from the aforementioned chelating adsorbates have been thoroughly characterized using a number of bulk and surface-sensitive techniques, including contact angle goniometry, ellipsometry, X-ray photoelectron spectroscopy (XPS), and polarization modulation infrared reflection absorption spectroscopy (PM-IRRAS).[17−23] These SAMs, however, have never been examined by electrochemical impedance spectroscopy (EIS), a popular electrochemical technique for acquiring important information regarding the electrical properties of coatings on metal surfaces.[24] Chemically adsorbed insulating films on metal surfaces are best represented by a Helmholtz ideal capacitor model (i.e., a parallel plate capacitor with a dielectric material).[25] A monolayer film that behaves as an ideal capacitor has a gold surface acting as one capacitor plate and physisorbed ions at the SAM/electrolyte interface acting as another capacitor plate. The intervening dielectric material is comprised largely of polymethylene groups (i.e., $-(CH_2)_n-$ repeat units). The capacitance of the SAM can be experimentally estimated based on the charging currents during cyclic voltammetry[26−28] or using EIS as reported more recently.[29−31]

Characterization of the interfacial properties of SAMs, especially under the influence of an applied potential, is essential for their fundamental study and their ultimate use in a variety of technological applications.[32−39] For example, SAMs prepared from long-chain alkanethiols serve as effective nanoscale electronic insulators in molecular electronic devices due to their relatively low conductivity, typically $5 \times 10^{-15}\ \Omega^{-1}\ cm^{-1}$.[32−35] However, as demonstrated by Whitesides and co-workers, the insulating properties of alkanethiolate SAMs can be readily

* To whom correspondence should be addressed. E-mail: radvincula@uh.edu (R.C.A.); trlee@uh.edu (T.R.L.).

10.1021/jp808957r CCC: $40.75 © 2009 American Chemical Society
Published on Web 02/06/2009

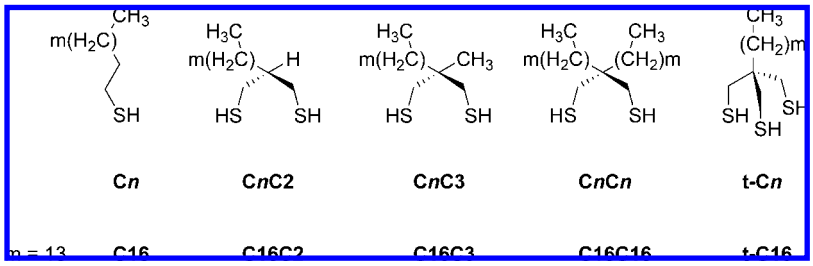

Figure 1. Structures of homologous bidentate and tridentate chelating thiols compared to normal hexadecanethiol.

degraded by electrolyte ions.[36] The ionic permeability is therefore a more useful measure of the insulating capacity of SAMs in electronic devices. In a related application, SAMs can be used to mimic phospholipid membranes with respect to their permeability. The effect of applied potential on SAMs provides valuable information regarding both membrane conductance and ionic translocation.[37] The electrical properties of SAMs are also important in their application as nanoscale inhibitors of corrosion. Both electric potential stability and ionic permeability strongly influence the corrosion-inhibiting ability of thin-film coatings on metal surfaces.[38,39]

In the work reported here, we use EIS to characterize the ionic insulating properties of SAMs on gold prepared from the series of adsorbates shown in Figure 1, where the packing density and conformational order of the films vary in a systematic manner. In contrast to previous studies in which electrochemically active redox species are used to probe the electron-transfer process,[29−31,40,41] we use an inert electrolyte solution containing no redox-active species; as a consequence, the electrochemical response of EIS in our system is governed by through-film processes, and heterogeneous charge transfer is highly impeded. Furthermore, we evaluate the electric potential stability of the SAMs based on voltammetric measurements of the reductive desorption of the adsorbates.[42−45] We also examine the ionic permeability under various applied cathodic potentials and/or at elevated temperatures. The influence of electric potential and thermal stability on the ionic permeability of the SAMs is discussed.

Experimental Section

Materials. 1-Hexadecanethiol (**C16**) was prepared from the commercially available bromide precursor and purified using chromatography on silica gel. 2-Tetradecylpropane-1,3-dithiol (**C16C2**), 2-tetradecyl-2-methylpropane-1,3-dithiol (**C16C3**), 2,2-ditetradecylpropane-1,3-dithiol (**C16C16**), and 1,1,1-tris-(mercaptomethyl)pentadecane (**t-C16**) were synthesized according to published procedures.[17−23]

Preparation of SAMs. A polycrystalline gold disk electrode (Bioanalytical Systems Inc.) with diameter of 1.6 mm was used as the substrate for SAM growth. The electrode was mechanically polished with a 50 nm alumina slurry on microcloth pads followed by sonication in pure water for 5 min to remove adhered alumina particles. The electrode was transferred into freshly prepared piranha solution (H_2SO_4:H_2O_2 = 3:1. **Caution:** *Piranha solution is highly corrosive and should be handled with care!*) for 3 min to remove any organic material on the electrode surface. After copious washing with distilled water, the electrode was further cleaned electrochemically in 0.1 M H_2SO_4 solution by cycling the potential between −0.45 and 1.1 V (vs Ag quasi-reference) at 500 mV/s. Finally, the electrode was thoroughly washed with deionized water (Milli-Q system, MA; 18 MΩ·cm) and absolute ethanol (200 proof).

The SAMs derived from **C-16**, **C16C2**, **C16C3**, and **C16C16** were prepared by immersing the freshly cleaned gold electrode into 1 mM ethanolic solutions of the appropriate thiol in a sealed glass container (e.g., vials), which were either thermally equilibrated at room temperature with the ambient environment or heated in an oil bath to 60 °C where indicated. Based on a previous study probing the optimal conditions for high quality SAM formation,[22,23] the SAM derived from **t-C16** was prepared either in tetrahydrofuran (THF) at room temperature or in both ethanol and isooctane at 60 °C. After equilibration for 48 h,[20] the electrode was removed from solution and carefully rinsed with copious amounts of absolute ethanol and deionized water prior to electrochemical characterization.

Impedance Measurements. Electrochemical impedance spectroscopy (EIS) measurements were conducted using a three-electrode configuration, where the gold electrode coated with a specific SAM was used as the working electrode coupled with a Ag/AgCl (aqueous solution of 3 M NaCl) reference electrode and a platinum coil auxiliary electrode. With the aid of a homemade Teflon cover, the electrodes were positioned in the electrochemical cell in a consistent manner to minimize the experimental variation. For collecting the impedance spectra, the testing bath utilized an aqueous solution of 50 mM potassium phosphate dibasic (K_2HPO_4, 99.99%, Aldrich) as the electrolyte.[29−31]

The impedance data were collected using a PARSTAT 2263 potentiostat/galvanostat (Princeton Applied Research). A sinusoidal potential modulation of 30 mV amplitude was superimposed on a constant dc potential during impedance measurements. After each measurement, the dc potential was cathodically increased in increments of 0.1 V. A series of impedance measurements with dc potentials from 0.4 to −0.7 V were conducted. The amplitude and the phase shift of the resulting current were recorded at each frequency from 100 kHz to 1 Hz. Thirty points, equally spaced on a logarithmic scale, were acquired per decade increment in frequency. The impedance data were iteratively fitted into a chosen equivalent electrical circuit using the complex nonlinear least squares (CNLS) immittance fitting program, giving the value of each component in the equivalent circuit.[46]

Cyclic Voltammetry. The reductive desorption of SAMs was performed in a 0.5 M KOH−ethanolic solution by potential cycling the working gold electrode from −0.5 to −1.5 V (vs Ag/AgCl) at 100 mV/s.[42] Prior to the voltammetry, the solution was purged with argon in a closed electrochemical cell for at least 5 min. The KOH−ethanolic solution was prepared fresh for each SAM analyzed.

Results and Discussion

Initial Ionic Permeability. The electric response of a SAM-modified electrode contacting an inert electrolyte solution can be described by an electric circuit, where the solution resistance, R_s, is in series with a constant phase element (CPE), as shown

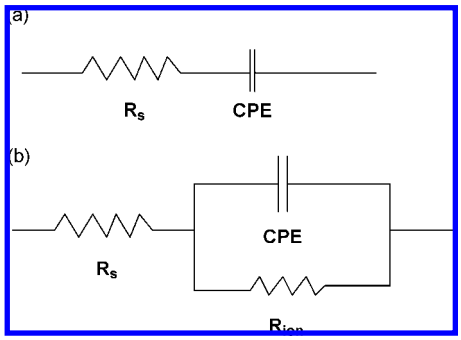

Figure 2. Generally accepted equivalent circuits of (a) a defect-free SAM and (b) a structurally imperfect SAM having defects/channels for ion transport. R_s = solution resistance, CPE = constant phase element representing the SAM, and R_{ion} = resistance of ion transport in the SAM.

in Figure 2a.[29−31] The impedance of the CPE is given by the following equation:

$$Z_{CPE} = A(j\omega)^{-\alpha} \quad (1)$$

where ω is the electric field frequency and both A and α are constants.[47] The value of α varies from 0 to 1 and reflects the ideality of the capacitor. When α equals 1.0, for example, the CPE is an ideal capacitor with a capacitance of A^{-1}. In reality, a small deviation from unity (e.g., $1 > \alpha > 0.88$) is always observed, even for a nearly perfect coating, and usually accounts for the topological imperfections of the polycrystalline gold surface caused by the different crystal facets and the surface roughness.[29−31]

The impedance spectra were acquired at a dc potential of 0 V (vs Ag/AgCl) in 50 mM K_2HPO_4 solution (pH 7−8) from a SAM-modified gold disk electrode, prepared by soaking in separate ethanolic solutions of 1-hexadecanethiol (**C16**), 2-tetradecylpropane-1,3-dithiol (**C16C2**), 2-tetradecyl-2-methylpropane-1,3-dithiol (**C16C3**), 2,2-ditetradecylpropane-1,3-dithiol (**C16C16**), and 1,1,1-tris(mercaptomethyl)pentadecane (**t-C16**) at room temperature for 48 h. The value of 0 V (vs Ag/AgCl) was chosen because an earlier study confirmed that organothiolates adsorbed on gold exhibit maximum stability at or near this potential.[48] The resulting impedance spectra were iteratively fitted to an equivalent serial RC circuit (Figure 2a) to determine the values of each component in the circuit. Figure 3 shows Bode plots and Nyquist plots of the impedance spectra. The fitting parameters are listed in Table 1.

Ideally, a Helmholtz capacitor should give a phase angle of 90° in a Bode phase plot (as a function of frequency),[47] while a perfect resistor has a phase angle of 0°. An imperfect capacitor or a circuit comprised of ideal capacitors and resistors gives a phase angle value between 0° and 90°. Deviation of the phase angle from 90° would suggest an electrical current leakage through or a bypass of the dielectric layer of the Helmholtz capacitor. In practical terms, however, a SAM with a phase angle slightly smaller than 90° in the low-to-mid-frequency range is still considered to be free of defects, meaning that current leakage, through either ionic channels or electronic conduction, is negligible or nonexistent. As shown in Figure 3a, Bode phase plots from the different SAMs show phase angles of ca. 80−88° at frequencies between 1 and 10^3 Hz, confirming the presence of a good insulating dielectric material on the electrode surface. At higher frequencies, the total impedance is dominated by the solution resistance, and the phase angle decreases toward zero.

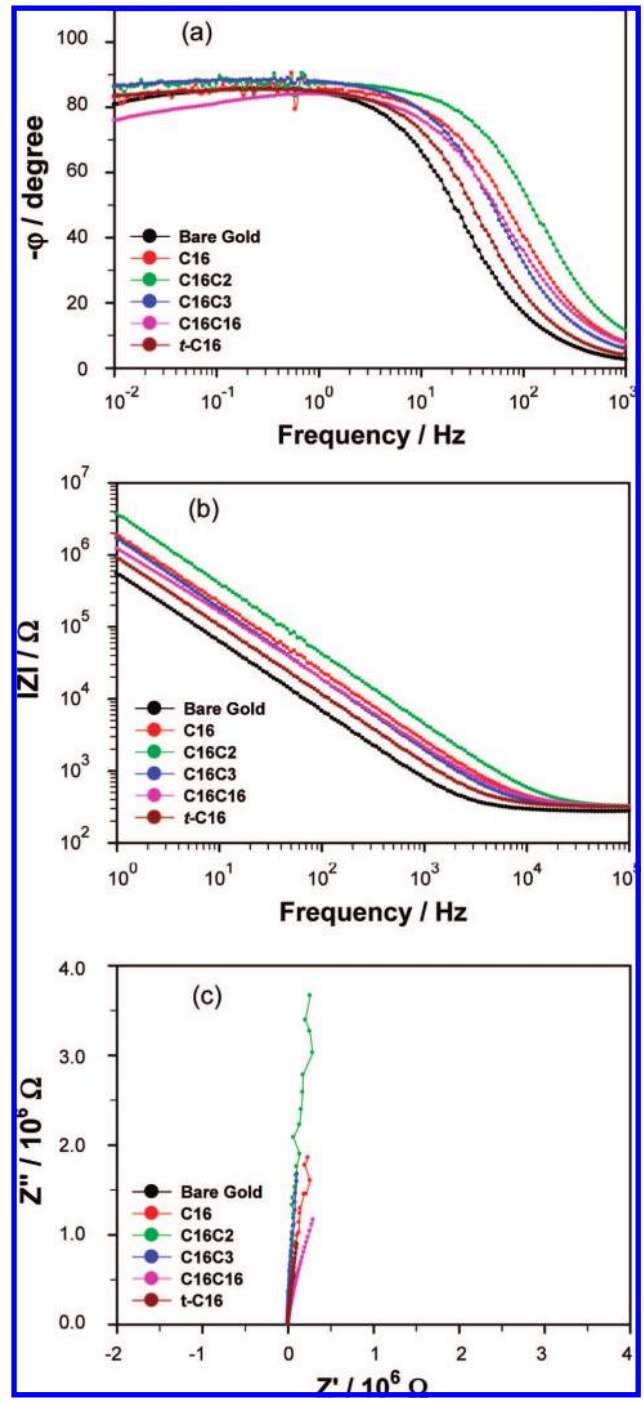

Figure 3. (a) Bode phase angles, (b) Bode magnitude, and (c) Nyquist plots for a bare gold disk (1.6 mm diameter) electrode surface and the indicated SAMs prepared by adsorption from ethanolic solution at room temperature on the electrode. The data were collected in 50 mM K_2HPO_4 solution under an applied dc potential of 0 V (vs Ag/AgCl) and a sinusoidal ac amplitude of 30 mV.

While confirming the capacitive effect arising from the dielectric coating on the electrode, the impedance at low frequency when the phase angle is near 90° gives inconclusive information regarding the ionic permeability of films since variations in the phase angle at low frequency are small (see Figure 3a), and the phase angle could be favorably influenced by the double-layer capacitance arising from the electrolyte solution contacting the metal surface through pinholes in the films.[49,50] Instead, the ionic permeability of the SAMs is more readily manifested in the relative magnitude of the film

TABLE 1: Fitting Parameters for CNLS Simulation of Impedance Spectra Obtained from the Indicated Samples[a]

SAM/Au	$R_s/\Omega\cdot cm^2$	CPE/$\mu F\cdot cm^{-2}$	α
bare gold	5.30 ± 0.03[b]	16.1 ± 0.1	0.947 ± 0.001
C16	6.01 ± 0.03	4.63 ± 0.03	0.947 ± 0.001
C16C2	6.07 ± 0.02	2.29 ± 0.01	0.968 ± 0.001
C16C3	6.05 ± 0.04	5.12 ± 0.05	0.967 ± 0.001
C16C16	6.03 ± 0.04	7.06 ± 0.06	0.920 ± 0.001
t-C16	6.11 ± 0.03	9.55 ± 0.07	0.947 ± 0.001

[a] The SAMs are equivalent to a defect-free, series RC circuit. [b] Estimated standard deviation of fitting parameters from CNLS simulation.

capacitance at lower frequencies, a time domain in which the measurements are more sensitive to slow ion transport through the film. A smaller capacitance value would suggest better impermeability of the film and can be further correlated to various structural factors, such as film thickness, packing structure, and dielectric properties. Given that the solution resistance always remains constant, the total impedance of the equivalent RC circuit gives a relative measure of film capacitance and provides direct evidence of the ionic permeability of the SAMs. The Bode plots obtained from the SAMs studied here (Figure 3b) show that the magnitude of the total impedance at 1 Hz, or impermeability of the films, follows the order **C16C2** > **C16** > **C16C3** > **C16C16** > **t-C16** > bare gold. Here, a frequency of 1 Hz represents the time domain for diffusion-related phenomena and was chosen to facilitate comparison of the various adsorbates.[51]

A more quantitative comparison of ionic permeability can be made by digitally simulating the experimental impedance spectra according to the simple series RC circuit shown in Figure 2a. The resulting fitting parameters are listed in Table 1. In most cases, we obtain good fitting of the data with a relative standard deviation of less than 1% for the fitting elements. The addition of an extra coating resistance (optional) in parallel to CPE gives a random fitting value of $>10^8$ ($\sim\infty$), suggesting that the film is essentially free of current leakage. A close review of the CPE values reveals that the capacitance of the SAMs follows the order **C16C2** < **C16** < **C16C3** < **C16C16** < **t-C16** < bare gold, which is the exact inverse of the order of the total impedance. We anticipated this result, given that the impedance of a capacitor is inversely proportional to its capacitance. The double-layer capacitance of the naked gold electrode is ca. 16 $\mu F\cdot cm^{-2}$, which is in good agreement with the values reported for polycrystalline gold surfaces in aqueous electrolyte solutions.[30,52]

By assuming a parallel plate capacitor model, the difference in capacitance can be ascribed to the ratio of the dielectric constant to the thickness of the SAM; both parameters are associated with the packing structure of the specific SAM prepared. Monolayers with higher packing density and conformational order, for example, might exhibit (1) a smaller dielectric constant due to the exclusion of polar solvent molecules from the hydrophobic surface, and (2) a thicker film due to a correspondingly smaller tilt angle.[12] Therefore, a more densely packed SAM with the same length of carbon chain should exhibit a smaller capacitance. Previous studies of SAMs formed from the thiol adsorbates in Figure 1 have determined that the packing density and conformational order follow the order **C*n*** > **C*n*C*n*** ≫ **C*n*C2** > **C*n*C3** > **t-C*n***.[17−23] This order is consistent with that of the impedance values obtained above, save for (1) **C16C2** having a greater impedance than both **C16** and **C16C16**, and (2) **C16C3** having a greater impedance than **C16C16**. It might be intuitive to attribute these inconsistencies

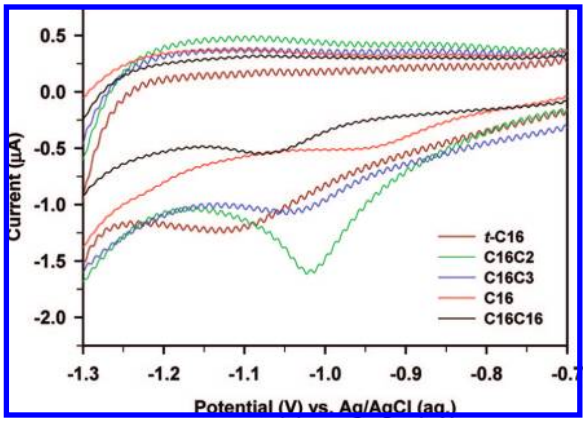

Figure 4. Cyclic voltammetry for reductive desorption of the indicated SAMs prepared by adsorption from ethanolic solution at room temperature on a 1.6-mm-diameter gold disk electrode. The data were collected in 0.5 M KOH−ethanolic solution by potential cycling a working gold electrode from −0.5 to −1.5 V (vs Ag/AgCl) at 100 mV/s. Prior to the voltammetry, the solution was purged with argon in a closed electrochemical cell for at least 5 min.

to the differing nature of the gold substrates used (i.e., bulk gold electrode vs evaporated gold on silicon wafers), given the complex and considerable influences on the structure of SAMs from topographic features of the underlying substrate such as surface roughness, crystallinity, and chemical surface pretreatment.[53−55] However, we tend to believe that the slight disorder of the loosely packed **C16C2** and **C16C3** SAMs might help eliminate defect sites present at domain boundaries in the more rigid, dense **C16** and **C16C16** SAMs,[17−23] leading to an enhanced impedance for the **C16C2** and **C16C3** SAMs, which is, however, diminished as the packing density decreases systematically for the **C16C2**, **C16C3**, and **t-C16** SAMs, respectively.

Figure 3c shows Nyquist plots of impedance spectra from the various SAMs. The plots exhibit a nearly vertical line parallel to the vertical axis over the entire frequency domain studied, typical of a series RC circuit.[47] Again, these data suggest that insignificant ion transport occurs through the SAMs during the current time scale of the experiments, and the films are essentially ionic insulators.

Electric Potential Stability. Organothiolates on metal surfaces undergo a chemical change in response to a sufficiently large electric potential. At highly positive and negative potentials in alkaline solutions, surface-bound organothiolates oxidatively or reductively desorb, forming sulfoxy and thiolate anions, respectively.[43−45] Here, we evaluate the electric potential stability of SAMs prepared from mono-, bi-, and tridentate thiols on gold substrates by examining their reductive desorption reactions: $Au-SR + e^- \rightarrow Au(0) + {}^-SR$. As shown in Figure 4, the electric current peaks, as a consequence of the breaking of Ag−S bonds and the subsequent desorption of thiols from the gold surface, are observed in the potential region from −0.9 to −1.1 V (vs Ag/AgCl). The potential where the desorption occurs measures how strongly the adsorbates can remain on the gold surface.[56] Examination of the desorption potentials indicates that the potential stability of the SAMs follows the sequence **C16** < **C16C2** ≈ **C16C3** ≈ **C16C16** < **t-C16**. Given that all the adsorbates bind through metal−sulfur bonds and possess alkyl tails of the same length, the observed trend is consistent with a model in which the adsorbate stabilities are dictated by the chelate effect:[20,57−59] that is, the tridentate thiols are more stably bonded to the surface of gold than the bidentate thiols, which are more stably bonded than the monodentate thiols. These

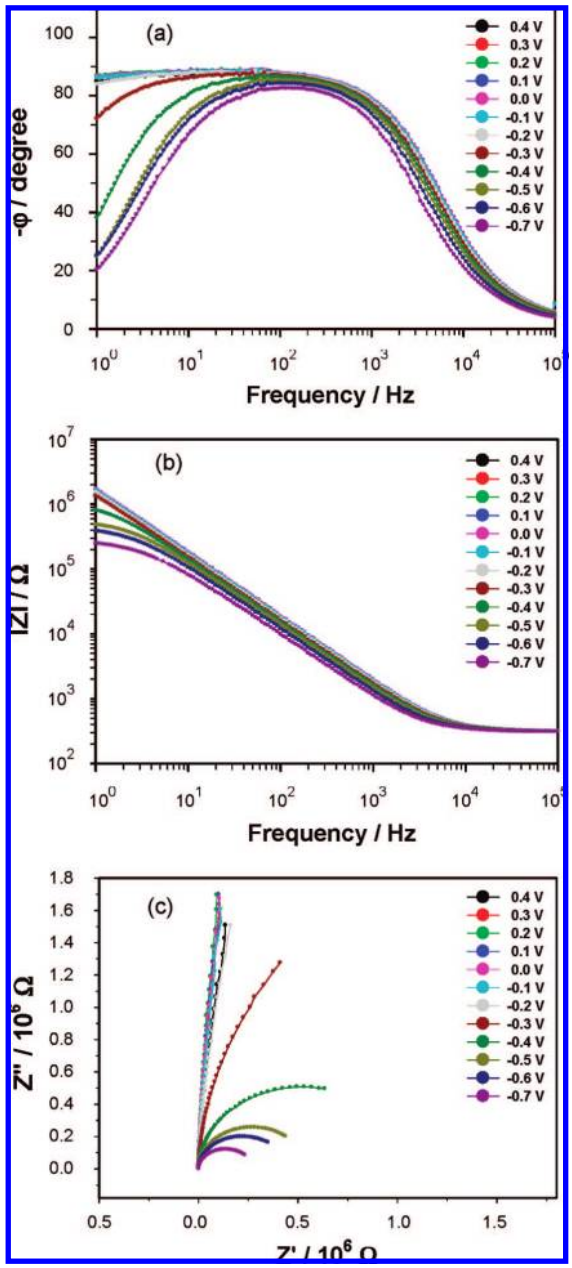

Figure 5. (a) Bode phase angles, (b) Bode magnitude, and (c) Nyquist plots for a bare gold disk (1.6 mm diameter) electrode surface and the **C16C3** SAM prepared by adsorption from ethanolic solution at room temperature on the electrode. The data were collected in 50 mM K_2HPO_4 solution under a varied dc potential from 0.4 V (vs Ag/AgCl) to −0.7 V and a sinusoidal ac amplitude of 30 mV.

results are consistent with our studies of the thermal stability of these adsorbates on both flat gold[23] and gold nanoparticles.[60]

Ionic Permeability under the Influence of Electric Potential. The influence of electric potential on the ionic permeability of SAMs can be probed in electrochemical impedance spectroscopy by varying the applied dc potential from +0.4 to −0.7 V in steps of 100 mV.[29−31] In this procedure, the impedance spectra are obtained at each incremental potential over a frequency range of 100 kHz to 1 Hz. The resultant data can then be used to generate Bode and Nyquist plots, such as those shown in Figure 5, which were obtained using **C16C3** as a typical adsorbate.

As demonstrated in Figure 5, the cathodic shift of the dc potential causes a dramatic change in the impedance spectra. First, as illustrated in Figure 5a, the phase angle at low frequency decreases from 88° at a potential of 0 V to 20° at a potential of −0.7 V. Given that the phase angle reflects the relative magnitude of the capacitive impedance and the solution resistance, a significant decrease of the phase angle suggests the occurrence of current leakage through the film. In other words, ionic transport through the SAM occurs to such an extent that the film can no longer be viewed as a pure capacitor. Consequently, the SAM cannot be accurately represented by an equivalent simple series RC circuit. Instead, we propose a more appropriate electric model, such as that shown in Figure 2b, to accommodate the current leakage through the film. Our proposed equivalent circuit is similar to that generally used to model the corrosion of a polymer-coated metal.[61] In our model, R_{ion} represents the ionic resistance in the defects or ionic channels of the SAM. Parallel to R_{ion} is CPE, which accounts for all capacitive effects associated with the gold surface.[29−31] We neglect the charge-transfer resistance due to the absence of the electrochemically active redox species in the range of potentials examined.

The impact of electric potential is also evident from the Bode plots (Figure 5b). The total impedance in the lower frequency range decreases and levels off to a constant value. The decrease of the total impedance can again be attributed to ionic penetration into the film and thus the breakdown of the capacitor. Considering that capacitors show higher impedance at lower frequencies, the total impedance levels off because most of the current flows through the resistors that are parallel to the capacitors. The extrapolation of the Bode plot into a frequency of 0 Hz should therefore reflect the combination of all resistance effects from the equivalent circuit. At much higher frequencies, all of the capacitors are electrically shorted due to the markedly lower impedance, and the circuit is essentially equivalent to the solution resistance. Apparently, all Bode plots level off to a constant value since the solution in every case contains the same concentration of electrolyte.

Figure 5c shows the Nyquist plots derived from **C16C3** at the various dc potentials examined. The plots change in shape from a vertical line to a semicircle when the potential is shifted to more cathodic values. While the vertical line of a Nyquist plot is characteristic of a simple series RC circuit, the semicircle shape is characteristic of a parallel RC circuit.[47] The observed evolution of the Nyquist plots indicates the development of a parallel electric current pathway, besides the capacitive effect, as a function of dc potential. Notice that the potentials explored here are substantially more anodic than the desorption potential of SAMs observed in cyclic voltammetry (−0.9 to −1.1 V). This potential-dependent change, while not fully excluding the contribution from desorption, most likely arises from a structural reorganization of film in coordination with the insertion of electrolyte ions under a constant dc potential gradient. The creation of more defects and the increased migration of ions into the film further influence the electrical response of the SAM in impedance spectra.

Plotting the phase angle at 1 Hz ($\varphi_{1\,Hz}$) vs the applied dc potential offers a qualitative illustration of the influence of the electric potential (see Figure 6a). When the potential is more positive of −0.1 V, the phase angles maintain a relatively constant value of ca. 80°, suggesting that both ionic penetration and structural changes in the film are minimal regardless of potential in this range. As the electric potential moves to more cathodic values, the phase angles from all of the SAMs decrease to much smaller angles. The observed decrease of the phase angles at low frequency, together with the noted observations in the Bode and Nyquist plots, indicates that the ionic perme-

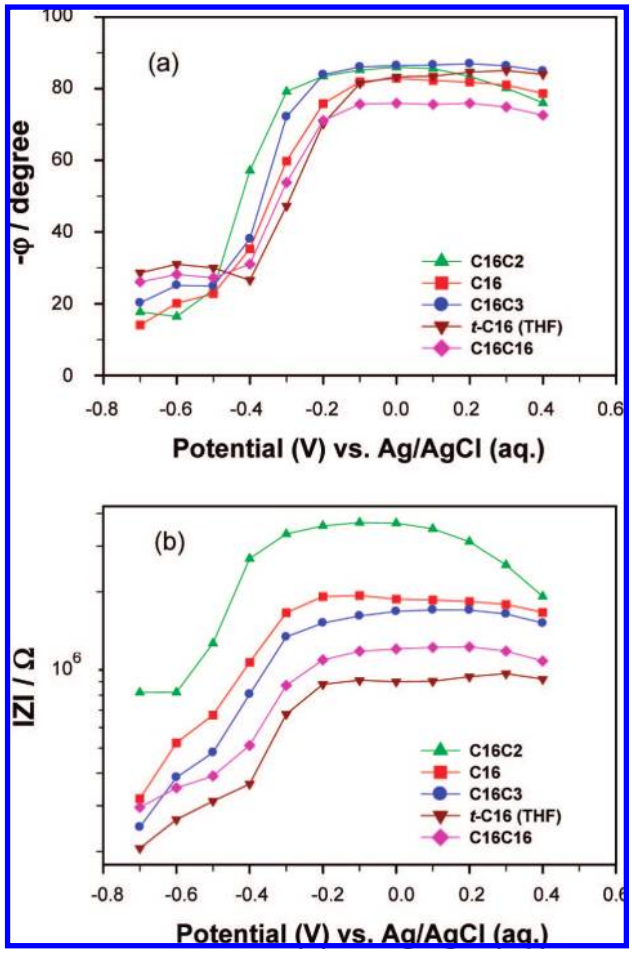

Figure 6. (a) Phase angles and (b) total impedance magnitude at 1 Hz acquired from impedance analysis of the indicated SAMs prepared by adsorption from ethanolic solution at room temperature onto a 1.6-mm-diameter gold disk electrode surface. EIS was conducted under a varied dc potential from 0.4 V (vs Ag/AgCl) to −0.7 V and a sinusoidal ac amplitude of 30 mV.

ability of the films degrades at reductive potentials. Importantly, the potential dependence of the degradation of the films varies with the nature of the adsorbate. As shown in Figure 6a, the SAM generated from **C16C2** is the most robust, where the phase angle at −0.4 V has decreased by only 34% from its initial value at 0 V. In contrast, the phase angle of the **t-C16** SAM decreases 69% over the same range of potentials. This observation suggests that the **C16C2** SAM maintains its ionic insulating properties well in response to the electric potential; consequently, this film should have a much greater capacity than the **t-C16** SAM to resist the penetration of ions. Based on the changes in the phase angles as a function of electric potential, the data in Figure 6a suggest that the ionic permeability of the SAMs at reductive electric potentials follows the order **C16C2** < **C16C3** < **C16** < **C16C16** < **t-C16**.

Interestingly, the initial ionic permeability obtained at ∼0 V gave a similar trend (i.e., **C16C2** < **C16** < **C16C3** < **C16C16** < **t-C16**; see Figure 3), differing only in the relative rankings of the **C16** and **C16C3** SAMs. It seems that the ionic permeability, which reasonably depends on the structure of the SAM, is also influenced by the potential stability of the SAM. As discussed above, the electric stability of SAMs is largely determined by the bonding between the adsorbate and the surface of gold. The tridentate adsorbate **t-C16** shows the strongest interaction with the metal surface (due to the three chelating Au−S bonds) and thus forms the most thermodynamically stable monolayer, which is followed by the bidentate adsorbates **C16C2**, **C16C3**, and **C16C16**, and then the monodentate adsorbate **C16**. The least stable **C16** SAM might undergo structural changes in response to the electric potential more so than the **C16C3** SAM, despite the fact that the initial quality of the **C16** SAM is better than that of the **C16C3** SAM. In contrast, the **t-C16** SAM, which is the most stable film under electric potential, possesses the highest ionic permeability in its initial state and is the least resistant to the penetration of ions at cathodic potentials.

Due to the observed dramatic change in the electric response of the SAMs as the potential is varied, two different equivalent circuits are required to simulate the impedance spectra. In the region where the film shows ionic insulating properties and the phase angle is above 80°, the film can be regarded as an ideal/near-ideal capacitor, and the data can thus be fitted by a simple series RC equivalent circuit as shown in Figure 2a. However, when the potential is shifted into the cathodic range where the phase angle drops below 80°, the film is permeable to electrolyte ions, and the film can no longer be viewed as an ideal capacitor. Instead, we use for the purpose of simulation the equivalent circuit shown in Figure 2b, where the defects in the film are represented by R_{ion} to describe ionic transport through the film. All simulation parameters are listed in Table 2.

The solution resistance, R_s, remains roughly constant during the set of experiments for each SAM prepared. The CPE elements represent mostly capacitive properties of the electrode surface since the index, α, is close to 1 in all cases.[47] The ionic permeability of the SAMs at different applied potentials is manifested by their capacitance. At potentials near 0 V where the SAMs are most stable, the values of capacitance are the smallest, and the films are the most resistant to the penetration of ions. In contrast, when the potential is shifted toward cathodic values, the capacitance and the ionic permeability increase. Given that the simulation in the cathodic region includes R_{ion} in the equivalent circuit, an increase in ionic transport will be reflected by a decrease in R_{ion}. At which potential R_{ion} should be included in the simulation depends on the response of the ionic permeability of an individual SAM to the electric potential. For example, the simulation of the **C16** SAM data at potentials of −0.2 V or higher gives a random fitting value of $>10^8$ (∼∞) with an unreasonably large standard deviation. A reproducible simulation of R_{ion} can be only achieved at potentials starting at −0.3 V and more cathodic. This potential can be regarded as the *critical potential*, where the SAMs begin to show significant permeability to ion transport, as similarly defined by Lennox.[29−31] When comparing films, a more negative critical potential is generally interpreted to indicate that a film is more resistant to potential-induced structural changes and has a lower ionic permeability. Following this criterion, a comparison of the critical potential from the various SAMs in Table 2 suggests the following order of ionic permeability at reductive potentials: **C16C2** ≈ **C16C3** (−0.4 V) < **C16** (−0.3 V) < **C16C16** ≈ **t-C16** (−0.2 V). This analysis is consistent with and thus provides support for the trend reported earlier in this section.

Ionic Permeability under the Influence of Thermal Stability. Previous reports have found that SAMs generated from bidentate and tridentate thiols (such as those examined here) are more thermodynamically stable than those generated from analogous monodentate normal alkanethiols; the thermal stability of the SAMs was observed to follow the sequence **t-C*n*** > **C*n*C2** ≈ **C*n*C3** ≈ **C*n*C*n*** > **C*n***.[17−23] The difference in stability was rationalized on the basis of the chelate effect.[17−23] One concern

TABLE 2: Fitting Parameters for CNLS Simulation of Impedance Spectra Obtained from the Indicated SAMs[a]

E/V (vs Ag/AgCl)	R_s/Ω·cm^2	CPE/μF·cm^{-2}	α	R_{ion}/MΩ
		C16		
+0.4	5.87 ± 0.04	5.02 ± 0.05	0.938 ± 0.001	*b*
+0.3	5.97 ± 0.03	4.78 ± 0.03	0.944 ± 0.001	*b*
+0.2	5.99 ± 0.03	4.73 ± 0.03	0.946 ± 0.001	*b*
+0.1	5.95 ± 0.04	4.73 ± 0.05	0.944 ± 0.001	*b*
0	6.01 ± 0.03	4.63 ± 0.03	0.947 ± 0.001	*b*
−0.1	5.99 ± 0.04	4.53 ± 0.04	0.949 ± 0.001	*b*
−0.2	5.99 ± 0.04	4.58 ± 0.04	0.949 ± 0.001	*b*
−0.3	5.97 ± 0.04	4.73 ± 0.04	0.947 ± 0.001	4.0 ± 0.2
−0.4	5.97 ± 0.04	4.93 ± 0.04	0.946 ± 0.001	1.41 ± 0.03
−0.5	5.95 ± 0.04	5.22 ± 0.05	0.944 ± 0.001	0.75 ± 0.01
−0.6	5.95 ± 0.04	5.67 ± 0.06	0.941 ± 0.001	0.57 ± 0.01
−0.7	5.91 ± 0.01	6.7 ± 0.2	0.933 ± 0.004	0.32 ± 0.01
		C16C2		
+0.4	6.01 ± 0.04	3.83 ± 0.03	0.925 ± 0.001	*b*
+0.3	6.01 ± 0.04	3.13 ± 0.02	0.942 ± 0.001	*b*
+0.2	6.07 ± 0.02	2.64 ± 0.01	0.958 ± 0.001	*b*
+0.1	6.01 ± 0.04	2.39 ± 0.02	0.964 ± 0.001	*b*
0	6.07 ± 0.02	2.29 ± 0.01	0.968 ± 0.001	*b*
−0.1	6.05 ± 0.02	2.29 ± 0.01	0.968 ± 0.001	*b*
−0.2	6.05 ± 0.02	2.34 ± 0.01	0.966 ± 0.001	*b*
−0.3	6.05 ± 0.02	2.49 ± 0.01	0.961 ± 0.001	*b*
−0.4	6.03 ± 0.02	2.69 ± 0.01	0.955 ± 0.001	5.7 ± 0.1
−0.5	6.03 ± 0.02	2.74 ± 0.02	0.954 ± 0.001	1.48 ± 0.01
−0.6	6.03 ± 0.02	2.79 ± 0.02	0.953 ± 0.001	0.882 ± 0.004
−0.7	6.03 ± 0.02	3.03 ± 0.02	0.948 ± 0.001	0.876 ± 0.004
		C16C3		
+0.4	5.99 ± 0.04	5.72 ± 0.06	0.961 ± 0.001	*b*
+0.3	6.03 ± 0.04	5.27 ± 0.05	0.966 ± 0.001	*b*
+0.2	6.05 ± 0.04	5.07 ± 0.05	0.967 ± 0.001	*b*
+0.1	5.97 ± 0.05	5.17 ± 0.05	0.964 ± 0.002	*b*
0	6.05 ± 0.04	5.12 ± 0.05	0.967 ± 0.001	*b*
−0.1	5.97 ± 0.05	5.47 ± 0.05	0.962 ± 0.002	*b*
−0.2	6.03 ± 0.04	5.72 ± 0.06	0.963 ± 0.001	*b*
−0.3	6.01 ± 0.04	6.27 ± 0.06	0.960 ± 0.001	*b*
−0.4	5.99 ± 0.04	6.82 ± 0.07	0.958 ± 0.001	0.110 ± 0.002
−0.5	5.99 ± 0.04	7.66 ± 0.08	0.954 ± 0.001	0.547 ± 0.005
−0.6	5.97 ± 0.04	9.25 ± 0.09	0.945 ± 0.001	0.438 ± 0.004
−0.7	5.93 ± 0.04	12.3 ± 0.1	0.932 ± 0.002	0.270 ± 0.003
		C16C16		
+0.4	5.91 ± 0.04	7.71 ± 0.06	0.910 ± 0.001	*b*
+0.3	5.97 ± 0.04	7.21 ± 0.06	0.916 ± 0.001	*b*
+0.2	5.99 ± 0.04	7.01 ± 0.06	0.919 ± 0.001	*b*
+0.1	6.00 ± 0.04	6.97 ± 0.06	0.920 ± 0.001	*b*
0	6.03 ± 0.04	7.06 ± 0.06	0.920 ± 0.001	*b*
−0.1	6.03 ± 0.04	7.21 ± 0.06	0.920 ± 0.001	*b*
−0.2	6.03 ± 0.04	7.56 ± 0.08	0.919 ± 0.001	4.6 ± 0.4
−0.3	6.03 ± 0.04	8.11 ± 0.08	0.917 ± 0.001	1.71 ± 0.05
−0.4	6.03 ± 0.05	8.86 ± 0.09	0.915 ± 0.002	0.64 ± 0.01
−0.5	6.01 ± 0.05	9.8 ± 0.1	0.914 ± 0.002	0.460 ± 0.005
−0.6	6.03 ± 0.05	10.8 ± 0.1	0.911 ± 0.002	0.417 ± 0.008
−0.7	6.01 ± 0.05	12.0 ± 0.1	0.910 ± 0.002	0.347 ± 0.007
		t-C16		
+0.4	6.09 ± 0.03	9.35 ± 0.07	0.950 ± 0.001	*b*
+0.3	6.11 ± 0.03	8.96 ± 0.07	0.953 ± 0.001	*b*
+0.2	6.11 ± 0.03	9.20 ± 0.06	0.950 ± 0.001	*b*
+0.1	6.11 ± 0.03	9.55 ± 0.07	0.947 ± 0.001	*b*
0	6.11 ± 0.03	9.55 ± 0.07	0.947 ± 0.001	*b*
−0.1	6.07 ± 0.03	9.55 ± 0.08	0.950 ± 0.001	*b*
−0.2	6.05 ± 0.04	9.50 ± 0.09	0.952 ± 0.001	3.5 ± 0.3
−0.3	6.03 ± 0.04	9.9 ± 0.1	0.952 ± 0.001	1.11 ± 0.03
−0.4	6.01 ± 0.04	11.1 ± 0.1	0.946 ± 0.001	0.423 ± 0.004
−0.5	5.91 ± 0.06	14.1 ± 0.3	0.928 ± 0.003	0.38 ± 0.01
−0.6	5.91 ± 0.04	16.4 ± 0.2	0.929 ± 0.002	0.333 ± 0.007
−0.7	6.01 ± 0.04	20.0 ± 0.2	0.919 ± 0.002	0.245 ± 0.002

[a] Two separate equivalent circuits were used, depending on the potential range probed. [b] A simple RC series equivalent circuit (Figure 2a) applies. Forced simulation according to parallel RC circuit (Figure 2b) gives a fitting value of >10^8 (∼∞) with a relative standard error from 10% to over 100%.

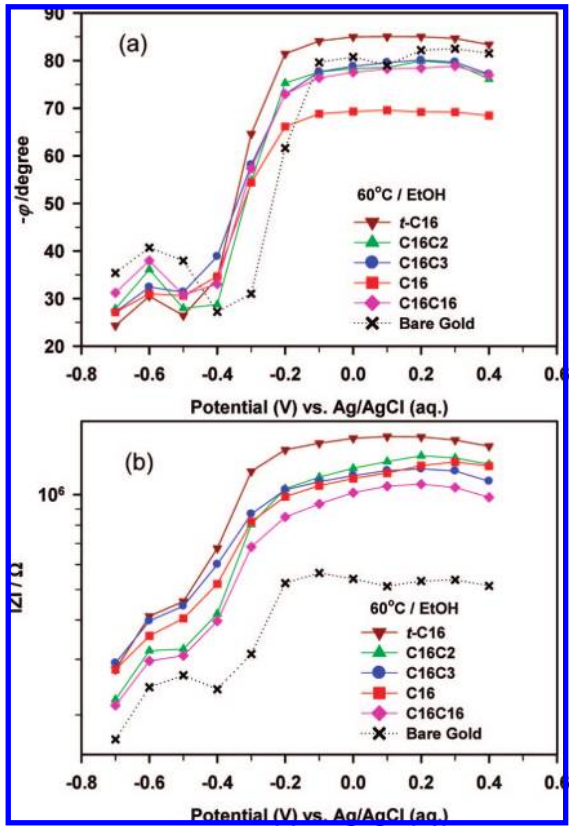

Figure 7. (a) Phase angles and (b) total impedance magnitude at 1 Hz acquired from impedance analysis of the indicated SAMs prepared by adsorption from ethanolic solution at 60 °C onto a 1.6-mm-diameter gold disk electrode surface. EIS was conducted under a varied dc potential from 0.4 V (vs Ag/AgCl) to −0.7 V and a sinusoidal ac amplitude of 30 mV.

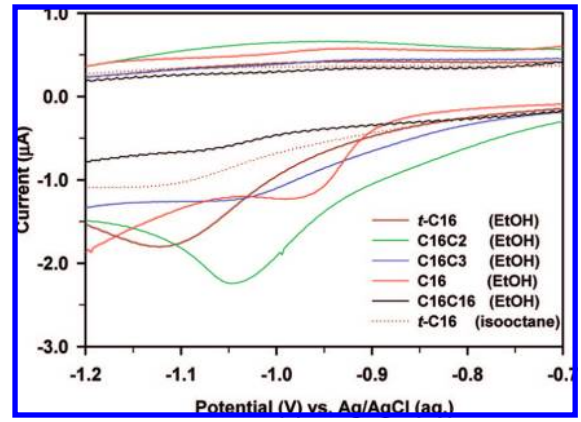

Figure 8. Cyclic voltammetry for reductive desorption of the indicated SAMs prepared by adsorption at 60 °C from indicated solvents onto a 1.6-mm-diameter gold disk electrode. The data were collected in 0.5 M KOH−ethanolic solution by potential cycling a working gold electrode from −0.5 to −1.5 V (vs Ag/AgCl) at 100 mV/s. Prior to the voltammetry, the solution was purged with argon in a closed electrochemical cell for at least 5 min.

regarding the preparation of SAMs from bidentate and tridentate thiols is whether a true equilibrium has been established at room temperature even after a 2-day adsorption process.[62] While the preparation of SAMs at elevated temperature expedites the equilibrium process, the effect of temperature on the stability of the SAMs comes into play, with more stable SAMs being generated at elevated adsorption temperatures.[20]

To examine further the influence of temperature on the adsorption process, we generated SAMs from the various thiols at 60 °C in ethanol and evaluated the insulating properties of the resulting films by electrochemical impedance spectroscopy. Figure 7 shows plots of the phase angles and the total impedance of the films as a function of potential. At potentials near 0 V, some differences in the phase angles can be discerned for the SAMs prepared from the different thiols; however, such parallel comparison is never conclusive in terms of the ionic permeability because the phase angles might be favored by the double-layer capacitance, especially if the quality of the SAMs formed at high temperature is poor (see Figure 2b). A better description of the ionic insulating properties again relies on the total impedance of the films. As illustrated in Figure 7b, the total impedance measured around 0 V for each monolayer follows the order **t-C16** > **C16C2** > **C16** ≈ **C16C3** > **C16C16**. Among them, the **t-C16** SAM has the least ionic permeability and thus the largest impedance to electric current.

The relative order of the ionic permeability of the SAMs prepared at elevated temperature is determined by both the initial permeability at room temperature and the thermal stability of the SAMs. As discussed above, the initial permeability of the SAMs follows the order **C16C2** < **C16** < **C16C3** < **C16C16** < **t-C16**, which is similar to the order obtained at 60 °C, except for **t-C16**. The **t-C16** SAM shows the best ionic insulating properties among all SAMs prepared at 60 °C despite its higher permeability at room temperature. Apparently, the adsorption of **t-C16** at elevated temperature leads to a film with enhanced thermal stability when compared to its adsorption at room temperature.[20]

The ionic permeability of SAMs prepared at 60 °C is also electric-potential dependent. The problem is simultaneously complicated by multiple factors: initial quality, thermal stability, and electric potential stability. Given the multiple crossovers in Figure 7, there are no simple trends that can be discerned with regard to ionic permeability at more cathodic potentials. However, the potential stability of the SAMs can still be determined by cyclic voltammetry. Figure 8 shows the desorption peaks measured for the various SAMs prepared at 60 °C. Based on the desorption potentials, the potential stability of the SAMs increases in the order **C16** < **C16C2** ≈ **C16C3** ≈ **C16C16** < **t-C16**, which is exactly the same trend found above for the films prepared at room temperature (see Figure 4). We note also that adsorptions from ethanol and isooctane give the same desorption potential for the **t-C16** SAM. The observation that potential stability is independent of temperature and solvent further supports our hypothesis that the potential stability is determined predominantly by the nature of the interaction between the adsorbate and the metal substrate (i.e., the degree of chelation).

Conclusions

The ionic permeability (or insulating) properties of SAMs prepared from monodentate, bidentate, and tridentate thiols having the same carbon chain length were probed by electrochemical impedance spectroscopy (EIS). The initial ionic permeability of the SAMs obtained at room temperature and evaluated by EIS under minimal electric potential bias shows that the ionic permeability increases as follows: **C16C2** < **C16** < **C16C3** < **C16C16** < **t-C16**. Furthermore, the ionic permeability of the films is influenced by the electric potential of the metal substrate and the temperature at which the SAMs were generated. Both the thermal and the electric potential stabilities of the SAMs follow the order **t-C16** > **C16C2** ≈ **C16C3** ≈

C16C16 > C16. The potential dependence of the ionic permeability of the various SAMs can be determined by considering both the initial ionic permeability and the potential stability. The resulting ionic permeability at more cathodic potentials follows the order **C16C2 < C16C3 < C16 < C16C16 < t-C16**. Similarly, the ionic permeability of the SAMs adsorbed at elevated temperature shows a contribution from an enhanced thermal stability in addition to the initial insulating properties of the films adsorbed at room temperature.

Acknowledgment. The Robert A. Welch Foundation (Grant E-1320) provided generous financial support for this research.

References and Notes

(1) Murray, R. W. *Acc. Chem. Res.* **1980**, *13*, 135.
(2) Lahann, J.; Mitragotri, S.; Tran, T.-N.; Kaido, H.; Sundaram, J.; Choi, I. S.; Hoffer, S.; Somorjai, G. A.; Langer, R. *Science* **2003**, *299*, 371.
(3) Bain, C. D.; Whitesides, G. M. *Science* **1998**, *240*, 62.
(4) Bain, C. D.; Whitesides, G. M. *J. Am. Chem. Soc.* **1989**, *111*, 7164.
(5) Bain, C. D.; Whitesides, G. M. *Angew. Chem.* **1989**, *101*, 522.
(6) Chen, S.; Li, L.; Boozer, C. L.; Jiang, S. *Langmuir* **2000**, *16*, 9287.
(7) Biebuyck, H. A.; Bain, C. D.; Whitesides, G. M. *Langmuir* **1994**, *10*, 1825.
(8) Higashi, N.; Takahashi, M.; Niwa, M. *Langmuir* **1999**, *15*, 111.
(9) Niwa, M.; Morikawa, M.-a.; Nabeta, T.; Higashi, N. *Macromolecules* **2002**, *35*, 2769.
(10) Choi, E. J.; Foster, M. D.; Daly, S.; Tilton, R.; Przybycien, T.; Majkrzak, C. F.; Witte, P.; Menzel, H. *Langmuir* **2003**, *19*, 5464.
(11) Choi, E. J.; Foster, M. D. *Langmuir* **2002**, *18*, 557.
(12) Jennings, G. K.; Munro, J. C.; Yong, T.-H.; Laibinis, P. E. *Langmuir* **1998**, *14*, 6130.
(13) Zamborini, F. P.; Campbell, J. K.; Crooks, R. M. *Langmuir* **1998**, *14*, 640.
(14) Zamborini, F. P.; Crooks, R. M. *Langmuir* **1998**, *14*, 3279.
(15) Kumar, A.; Biebuyck, H.; Whitesides, G. M. *Langmuir* **1994**, *10*, 1498.
(16) Xia, Y.; Whitesides, G. M. *Angew. Chem., Int. Ed.* **1998**, *37*, 550.
(17) Shon, Y.-S.; Colorado, R., Jr.; Williams, C. T.; Bain, C. D.; Lee, T. R. *Langmuir* **2000**, *16*, 541.
(18) Lee, S.; Shon, Y.-S.; Colorado, R., Jr.; Guenard, R. L.; Lee, T. R.; Perry, S. S. *Langmuir* **2000**, *16*, 2220.
(19) Shon, Y.-S.; Lee, S.; Colorado, R., Jr.; Perry, S. S.; Lee, T. R. *J. Am. Chem. Soc.* **2000**, *122*, 7556.
(20) Shon, Y.-S.; Lee, T. R. *J. Phys. Chem. B* **2000**, *104*, 8192.
(21) Shon, Y.-S.; Lee, S.; Perry, S. S.; Lee, T. R. *J. Am. Chem. Soc.* **2000**, *122*, 1278.
(22) Park, J.-S.; Smith, A. C.; Lee, T. R. *Langmuir* **2004**, *20*, 5829.
(23) Park, J.-S.; Nguyen Vo, A.; Barriet, D.; Shon, Y.-S.; Lee, T. R. *Langmuir* **2005**, *21*, 2902.
(24) Finklea, H. O. Electrochemistry of Organized Monolayers of Thiols and Related Molecules on Electrodes. In *Electroanalytical Chemistry*, Bard, A. J., Rubinstein, I., Eds.; Marcel Dekker: New York, 1996; Vol. 19, pp 109−335.
(25) Helmholtz, H. *Ann. Phys.* **1879**, *7*, 337.
(26) Finklea, H. O.; Avery, S.; Lynch, M. *Langmuir* **1987**, *3*, 409.
(27) Porter, M. D.; Bright, T. B.; Allara, D. L.; Chidsey, C. E. D. *J. Am. Chem. Soc.* **1987**, *109*, 3559.
(28) Chidsey, C. E. D.; Loiacono, D. N. *Langmuir* **1990**, *6*, 682.
(29) Boubour, E.; Lennox, R. B. *J. Phys. Chem. B* **2000**, *104*, 9004.
(30) Boubour, E.; Lennox, R. B. *Langmuir* **2000**, *16*, 4222.
(31) Boubour, E.; Lennox, R. B. *Langmuir* **2000**, *16*, 7464.
(32) Mann, B.; Kuhn, H. *J. Appl. Phys.* **1971**, *42*, 4398.
(33) Boulas, C.; Davidovits, J. V.; Rondelez, F.; Vuillaume, D. *Phys. Rev. Lett.* **1996**, *76*, 4797.
(34) Vuillaume, D.; Boulas, C.; Collet, J.; Davidovits, J. V.; Rondelez, F. *Appl. Phys. Lett.* **1996**, *69*, 1646.
(35) Rampi, M. A.; Schueller, O. J. A.; Whitesides, G. M. *Appl. Phys. Lett.* **1998**, *72*, 1781.
(36) Hagg, R.; Rampi, M. A.; Holmlin, R. E.; Whitesides, G. M. *J. Am. Chem. Soc.* **1999**, *121*, 7895.
(37) Badia, A.; Back, R.; Lennox, R. B. *Angew. Chem., Int. Ed. Engl.* **1994**, *33*, 2333.
(38) Laibinis, P. E.; Whitesides, G. M. *J. Am. Chem. Soc.* **1992**, *114*, 9022.
(39) Jennings, G. K.; Laibinis, P. E. *Colloids Surf., A* **1996**, *116*, 105.
(40) Finklea, H. O.; Snider, D. A.; Fedyk, J.; Sabatani, E.; Gafni, Y.; Rubinstein, I. *Langmuir* **1993**, *9*, 3660.
(41) Zhao, M.; Zhou, Y.; Bruening, M. L.; Bergbreiter, D. E.; Crooks, R. M. *Langmuir* **1997**, *13*, 1388.
(42) Everett, W. R.; Fritsch-Faules, I. *Anal. Chim. Acta* **1995**, *307*, 253.
(43) Widrig, C. A.; Chung, C.; Porter, M. D. *J. Electroanal. Chem.* **1991**, *310*, 335.
(44) Walczak, M. M.; Popenoe, D. D.; Deinhammer, R. S.; Lamp, B. D.; Chung, C.; Porter, M. D. *Langmuir* **1991**, *7*, 2687.
(45) Weisshaar, D. E.; Lamp, B. D.; Porter, M. D. *J. Am. Chem. Soc.* **1992**, *114*, 5860.
(46) Macdonald, J. R. In *Complex Nonlinear Least Squares Immittance Fitting Program, LEVM 7.0*; Macdonald, J. R., Ed.; Department of Physics and Astronomy, University of North Carolina: Chapel Hill, NC, 1990.
(47) Macdonald, J. R. *Impedance Spectroscopy*; Wiley: New York, 1987.
(48) Everett, W. R.; Welch, T. L.; Reed, L.; Fritsch-Faules, I. *Anal. Chem.* **1995**, *67*, 292.
(49) Yamamoto, Y.; Nishihara, H.; Aramaki, K. *J. Electrochem. Soc.* **1993**, *140*, 436.
(50) Feng, Y.; Teo, W.-K.; Siow, K.-S.; Gao, Z.; Tan, K.-L.; Hseih, A.-K. *J. Electrochem. Soc.* **1997**, *144*, 55.
(51) Janek, R. P.; Fawcett, W. R.; Ulman, A. *J. Phys. Chem. B* **1997**, *101*, 8550.
(52) Swietlow, A.; Skoog, M.; Johansson, G. *Electroanalysis* **1992**, *4*, 921.
(53) Creager, S. E.; Hockett, L. A.; Rowe, G. K. *Langmuir* **1992**, *8*, 854.
(54) Guo, L.; Facci, J. S.; McLendon, G.; Mosher, R. *Langmuir* **1994**, *10*, 4588.
(55) Leopold, M. C.; Black, J. A.; Bowden, E. F. *Langmuir* **2002**, *18*, 978.
(56) Bard, A. J.; Faulkner, L. R. *Electrochemical Methods Fundamentals and Applications*; John Wiley & Sons, Inc.: New York, NY, 2001.
(57) The free energy (ΔG) contribution of chelate effect is on the order of ~ -4 kcal/mol at room temperature assuming $\Delta H \sim -2$ kcal/mol and $\Delta S \sim +7$ cal/(K·mol).[58]
(58) Dubois, L. H.; Zegarski, B. R.; Nuzzo, R. G. *J. Am. Chem. Soc.* **1990**, *112*, 570.
(59) Huheey, J. E. *Inorganic Chemistry*; Harper Collins: Singapore, 1983.
(60) Zhang, S.; Leem, G.; Srisombat, L.; Lee, T. R. *J. Am. Chem. Soc.* **2008**, *130*, 113.
(61) Mitton, D. B.; Latanision, R. M.; Bellucci, F. *J. Electrochem. Soc.* **1996**, *143*, 3307.
(62) Xu, S.; Gruchon-Dupeyrat, S. J. N.; Garno, J. C.; Liu, G.-Y.; Jennings, G. K.; Yong, T.-H.; Laibinis, P. E. *J. Chem. Phys.* **1998**, *108*, 5002.

JP808957R